Cellular patterns produced by the directional solidification of a binary-alloy

Gregory Dee
Institute for Theoretical Physics, University of California at Santa Barbara, Santa Barbara, California 93106

Rajiv Mathur
Intel Corporation, 3065 Bowers Avenue, Santa Clara, California 95051

(Received 31 January 1983)

We develop a realistic model of directional solidification of a binary-alloy. We analyze the model in a one-dimensional (thin-film sample) geometry and find that the solidification interface undergoes a transition from a planar interface to a smooth cellular interface. We investigate the nature and stability of these states as functions of the parameters of the model. We find that smooth cellular states only exist close to the marginal stability point.

I. INTRODUCTION

Certain dynamical systems undergo pattern-forming transitions. Examples of such phenomena can be found in nonequilibrium situations such as directional solidification[1,2] of alloys, Rayleigh-Bénard convection,[3] and other hydrodynamic, biological, and chemical processes. In these systems, the observed patterns seem to lie in a small subset of the total set of possible states. In this paper we work with a realistic model of directional solidification in binary-alloy thin-film samples which exhibit pattern formation. We also investigate the nature and stability of such patterns as functions of the parameters of the model.

The system we wish to consider is shown in Fig. 1. It consists of a thin film of a binary alloy which is being moved at a constant velocity v in the negative z direction through a temperature gradient $\bar{G}$ created by the hot and cold contacts at A and B, respectively. The temperature gradient is such that the film is in the solid phase at B and in the liquid phase at A. The solidification interface is shown separating the two phases, and it is this interface that can undergo pattern-forming transitions.

In experiments done on such systems,[2] it is observed, that on increasing the value of a parameter $\bar{v}$, which is proportional to the velocity v and inversely proportional to the temperature gradient $\bar{G}$, the solidification interface undergoes a transition from a planar configuration to a periodic cellular configuration at a critical value of $\bar{v}$ equal to $\bar{v}_c$. The size of these cells varies from 10 to 100 μm. It is observed that for $\bar{v}$ close to $\bar{v}_c$, these cellular patterns are dominated by a fundamental wave vector $\vec{k}_c$. If $\bar{v}$ is increased still further, the system exhibits more complicated cellular patterns. For still higher values of $\bar{v}$, solidification proceeds by the formation of dendritic structures. We are interested in developing techniques to analyze our model in the vicinity of $\bar{v}_c$ where we expect cellular patterns.

The problem is nonlinear in character; the first systematic study of the nonlinear problem was performed by Wollkind and Segel,[4] who used a small parameter-expansion technique to investigate the small-amplitude stationary states near the region of neutral stability. They concluded from their analyses that stable periodic states can only be expected for very dilute alloys. Their analysis, however, is restricted to the close vicinity of the neutral stability point at $\bar{v}=\bar{v}_c$, and we would like to probe further into the nonlinear domain for which the planar interface is unstable. Strassler and Schneider[5] have obtained a set of integral equations for the interfa-

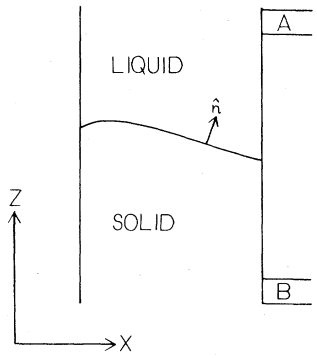

FIG. 1. Binary-alloy sample solidifying in the positive direction where $\hat{n}$ is the unit vector normal to the surface.

cial motion but have not carried out a nonlinear analysis of these equations. Nash[6] has also applied integral-equation methods to the study of solidification in binary eutectic solid solutions.

This paper is the third in a series on interfacial stability. In the preceding two papers (hereafter referred to as I and II), a "symmetric model" was studied for two different physical situations. In I,[7] the average position of the interface was kept fixed. In II,[8] the average position of the interface moved with a constant velocity as in the directional solidification technique. The symmetric model is so called because the coefficients of solute diffusivity in both phases are equal. Thus this model, while incorporating many of the features of the problem, is not a realistic model of a liquid-solid solidification interface. However, the Green's-function technique used in I and II will be used in this paper to derive the equation of motion for the interface. We shall introduce a "moving one-sided model" similar to the moving symmetric model (described in II). In this model we will assume that the coefficient of solute diffusivity is zero in the solid phase. Other features of the model include different thermal conductivities in the two phases and a variable miscibility gap. The model is described in detail in Sec. II. It is a realistic model of directional solidification and hence allows for the possibility of comparison of our results with experiments.

An outline of this paper is as follows: In Sec. II we describe the one-sided model. Section III is devoted to the derivation of the integro-differential equation which describes the dynamic behavior of the interface. We introduce an expansion scheme in Sec. IV which enables us to look for stationary solutions in the limit of small interfacial deformations. We investigate the stability of the planar interface. This stability analysis reveals the presence of a slow mode for $\bar{v}$ close to $\bar{v}_c$ which has a wave vector close to $\vec{k}_c$. In Sec. V we discuss an approach to the analysis of stationary stable states for $\bar{v}$ close to $\bar{v}_c$. We express the interfacial position as a Fourier series and we derive the equations of motion for the amplitudes of this series. We then assume the presence of a slow mode which allows us to solve these equations, assuming that there is a dominant amplitude or pair of amplitudes. This method, while not being mathematically elegant, allows us to probe the nonlinear domain of $\bar{v} \geq \bar{v}_c$. In Sec. VI we present the details of the stability analysis of the stationary states of the model. We investigate the stability of our solutions against perturbations which destroy the long-range periodicity of these solutions. Section VII is devoted to the results of applying the techniques outlined in Secs. V and VI to the moving one-sided model. We find that stable periodic solutions for the interface displacement exist in a domain of $\bar{v}$ above $\bar{v}_c$, and we investigate the size of this domain as a function of the other parameters of the model. We find that, within this domain, the amplitude of the periodic solution never grows larger than about 20% of the wavelength of the periodic state. Beyond this domain, that is, for $\bar{v}$ greater than some $\bar{v}_f > \bar{v}_c$, the smooth periodic solutions cease to exist and, presumably, the interface displacement becomes cusplike or dendritic. Our analysis cannot be extended to the latter cases.

II. ONE-SIDED MODEL

The one-sided model is similar to the model employed by Mullins and Sekerka.[9] The system is characterized by a composition field $C(\vec{x},t)$ and a temperature field $T(\vec{x},t)$ in the liquid phase. The corresponding fields in the solid phase will be denoted by $C'(\vec{x},t)$ and $T'(\vec{x},t)$. The physical situation we wish to consider is shown schematically in Fig. 1. As in the symmetric model, the solid phase is growing in the positive z direction with a constant velocity v. We shall assume that a large-scale steady state has been reached, so that the composition field approaches a fixed value C_0 in both directions ($\pm z$) away from the interface. We will neglect the effects of convection and interface attachment kinetics. We will also assume that the effect of the latent heat of fusion is negligible.

The model assumes the form of the phase diagram shown in Fig. 2. The solidus and liquidus are straight lines. The ratio of the slope of the liquidus to that of the solidus is the partition coefficient κ, which is assumed to be fixed for a given alloy. Solute diffusion in the solid is assumed to be negligible compared to that in the liquid; therefore, we will set the value of the solute diffusivity equal to zero in the solid phase. The temperature of a steady-state planar interface T_0 is specified by the intercept of a

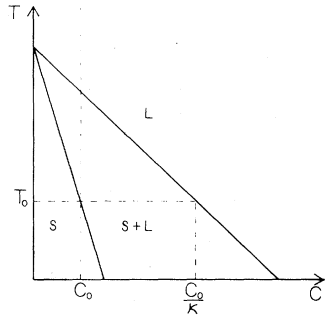

FIG. 2. Typical phase diagram for a binary alloy. The upper solid line is the solidus and the lower solid line is the liquidus. The two-phase region lies between these two lines. C_0 is the solute concentration in the solid.

vertical line at C_0 with the solidus as shown in Fig. 2. The composition difference between the adjacent solid and liquid phases is $\Delta C_0 = C_0(1/\kappa - 1)$. For the nonplanar interface, the temperature at a point on the interface is determined by the configuration of the interface at that point.

The temperature fields in both phases are assumed to be in a quasisteady state and satisfy Laplace's equation. This assumption is justified by the fact that thermal diffusivities are several orders of magnitude larger than chemical diffusivities, so that the temperature fields relax very quickly to their steady-state values.

There are three characteristic lengths in this model. The length describing the range of the solute diffusion field is defined as

$$l = \frac{2D}{v} , \tag{2.1}$$

where D is the coefficient of solute diffusivity in the liquid. There is also a length scale associated with the temperature field which is

$$l_T = \frac{|m|\Delta C_0}{G} , \tag{2.2}$$

where m is the slope of the liquidus and G is the temperature gradient in the liquid for a planar interface. We can also define an average thermal length $\bar{l}_T$ which is

$$\bar{l}_T = \frac{|m|\Delta C_0}{\bar{G}} , \tag{2.3}$$

where

$$\bar{G} = \frac{K_S G' + K_L G}{K_S + K_L}$$

is the weighted average of the temperature gradients in the solid and liquid phases, and $K_S(K_L)$ is the thermal conductivity of the solid (liquid) phase. The third length scale in the problem is associated with the Gibbs-Thomson surface-tension correction at a curved interface; we define a capillary length as follows:

$$d_0 = \frac{T_m \gamma}{|m|\Delta C_0 L} , \tag{2.4}$$

where γ is the surface tension at the interface, L is the latent heat of melting, and T_m is the melting temperature of the pure material. If we scale all lengths of the problem with the diffusion length l, we can characterize the system by the following dimensionless ratios:

$$\nu = \frac{l_T}{l} ,$$

$$\bar{\nu} = \frac{\bar{l}_T}{l} ,$$

and

$$\xi = \frac{d_0}{l} . \tag{2.5}$$

We will also define new composition and thermal fields by the following definitions:

$$u = \frac{C - C_0}{\Delta C_0} , \tag{2.6a}$$

$$\theta = \frac{T - T_0}{|m|\Delta C_0} - \frac{z}{\nu l} , \tag{2.6b}$$

and

$$\theta' = \beta \left[\frac{T' - T_0}{|m|\Delta C_0} \right] - \frac{z}{\nu l} , \tag{2.6c}$$

where

$$\beta = \frac{K_S}{K_L} .$$

We can now write down the basic equations for the system in terms of the variables defined in (2.6). We will scale all times with the quantity l^2/D and we will consider the situation where we are in a moving frame moving at a fixed velocity v in the z direction. The equations of motion for the fields u and θ are

$$\tilde{\nabla}^2 u + 2\frac{\partial u}{\partial \tilde{z}} = \frac{\partial u}{\partial \tilde{t}} \tag{2.7}$$

and

$$\tilde{\nabla}^2 \theta = \tilde{\nabla}^2 \theta' = 0 , \tag{2.8}$$

where the tildes denote scaled quantities, i.e., $\tilde{z} = z/l$ and $\tilde{t} = tD/l^2$. In the following discussions we will drop the tilde notation with the understanding that all lengths and times have been scaled as described above. The position of the interface is then given by

$$z = \zeta(\vec{x}, t) . \tag{2.9}$$

The conditions for heat and solute flux conservation are expressed by the following equations:

$$(\vec{\nabla}\theta' - \vec{\nabla}\theta)_{\text{int}} \cdot \vec{n} = 0 \tag{2.10a}$$

and

$$(-\vec{\nabla} u \cdot \vec{n})_{\text{int}} = \left[2 + \frac{d\zeta}{dt} \right] [\kappa + (1-\kappa) u_{\text{int}}] , \tag{2.10b}$$

where the subscript int indicates that the variable is to be evaluated at the interface. The vector $\vec{n}$ is the unit normal at the interface as indicated in Fig. 1. The thermodynamic boundary conditions at the interface are

$$\theta_{\rm int}=1-u_{\rm int}+\xi\mathscr{K}(\zeta)-\zeta/\bar{v}\ , \tag{2.11}$$

$$\theta'_{\rm int}=\beta[1-u_{\rm int}+\xi\mathscr{K}(\zeta)]-\zeta/\bar{v}\ , \tag{2.12}$$

where $\mathscr{K}(\zeta)$ is the local interfacial curvature and is given by the following expression:

$$\mathscr{K}(\zeta)=\frac{\nabla^2\zeta}{[1+(\vec{\nabla}\zeta)^2]^{3/2}}\ . \tag{2.13}$$

Finally, the boundary conditions at $|z|=\infty$ are as follows:

$$u(z\to\infty)=0\ , \tag{2.14a}$$

$$\frac{d\theta}{dz}(z\to\infty)=0\ , \tag{2.14b}$$

and

$$\frac{d\theta'}{dz}(z\to-\infty)=0\ . \tag{2.14c}$$

In terms of these new fields u and θ, the planar interface solution ($\zeta=0$) of Eqs. (2.7) and (2.8) with the above boundary conditions is

$$\theta=\theta'=0\ , \tag{2.15a}$$

$$u=e^{-2z}\ , \tag{2.15b}$$

$$u'=0\ . \tag{2.15c}$$

III. DERIVATION OF THE EQUATION OF MOTION

Following the scheme introduced in papers I and II of this series, we will employ a Green's-function technique[8,10] to obtain a pair of integral equations which we will use to derive an equation for the interfacial displacement $\zeta(\vec{x},t)$. We will consider the thermal field first and we will obtain a relationship which can later be used to eliminate $u_{\rm int}$ from the solution for the solute diffusion field u. We begin by writing the Green's function for the Laplace equation,

$$G_\theta(\vec{r},\vec{r}_1)=\frac{1}{4\pi|\vec{r}-\vec{r}_1|}\ , \tag{3.1}$$

which satisfies

$$\nabla_1^2 G_\theta(\vec{r},\vec{r}_1)=-\delta(\vec{r}-\vec{r}_1)\ . \tag{3.2}$$

Multiplying (3.2) by $\theta(\vec{r}_1)$ and integrating over a volume v_L whose surface is S_L (as shown in Fig. 3), we obtain

$$\theta(\vec{r})=-\int_{S_L}[\theta(\vec{r}_1)\vec{\nabla}_1 G_\theta(\vec{r},\vec{r}_1) - G_\theta(\vec{r},\vec{r}_1)\vec{\nabla}_1\theta(\vec{r}_1)]\cdot\vec{n}\,dS_1\ , \tag{3.3}$$

where we have used Green's second theorem. By allowing the outer part of the surface S_L to go to infinity and the lower part approach the interface, the only contributions to the integral (3.3) will come from the interface. Allowing the point $\vec{r}$ approach the interface, we obtain

$$\theta(\vec{r}_{\rm int})=\int_{\rm int}\theta(\vec{r}_1^{\rm int})\frac{[(\zeta-\zeta_1)-\vec{\nabla}_1\zeta_1\cdot\Delta\vec{x}]d^2x_1}{4\pi[(\Delta\vec{x})^2+(\zeta-\zeta_1)^2]^{3/2}}-\int_{\rm int}G_\theta(\vec{r}^{\,\rm int},\vec{r}_1^{\,\rm int})\vec{\nabla}_1\theta(\vec{r}_1^{\,\rm int})\cdot\vec{n}\,dS_1\ , \tag{3.4}$$

where $\Delta\vec{x}=\vec{x}-\vec{x}_1$. Repeating the above procedure in the solid phase, we obtain a similar expression for $\theta'(\vec{r}_{\rm int})$ with the signs on both terms in (3.4) reversed. Adding these two equations and using (2.10a), (2.11), and (2.12), we get

$$w(\vec{x})=\psi(\beta)f\left[w(\vec{x}_1)+\frac{\zeta_1}{\bar{v}}\right]\ , \tag{3.5}$$

where we have introduced the following notation:

$$w(x)=1-u_{\rm int}+\xi\mathscr{K}(\zeta)-\zeta/\bar{v}\ , \tag{3.6a}$$

$$f[w]=\int d^2\vec{x}_1\frac{[(\zeta-\zeta_1)-\vec{\nabla}_1\zeta_1\cdot(\vec{x}-\vec{x}_1)]}{4\pi[(\vec{x}-\vec{x}_1)^2+(\zeta-\zeta_1)^2]^{3/2}}w(\vec{x}_1)\ , \tag{3.6b}$$

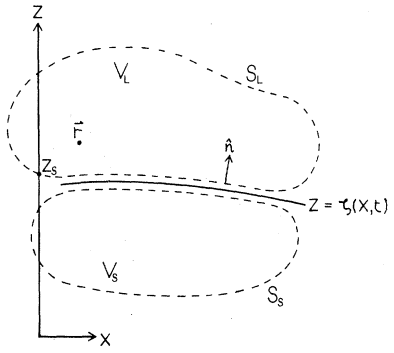

FIG. 3. Solidification interface $z=\zeta(x,t)$ is shown separating the volumes V_s and V_L whose surfaces are S_s and S_L, respectively.

and

$$\psi(\beta)=\frac{1-\beta}{1+\beta} . \tag{3.6c}$$

In deriving Eq. (3.5), we have used the fact that

$$1/\bar{\nu}=\frac{2}{\nu(1+\beta)} . \tag{3.6d}$$

Equation (3.5) is an integral equation in the unknowns $u_{\rm int}$ and $\zeta(\vec{x},t)$.

Our next step is to use (3.5) to generate an expansion for $u_{\rm int}$ in powers of ζ. It is convenient to use a Fourier representation to accomplish this. Formally, we write

$$\hat{w}(k,\omega)=\sum_{m=2}^{\infty}\int\frac{d^2k_1}{(2\pi)^2}\int\frac{d^2k_2}{(2\pi)^2}\int\frac{d\omega_1}{2\pi}\int\frac{d\omega_2}{2\pi}W^{(m)}(\vec{k},\vec{k}_1,\vec{k}_2,\ldots,\vec{k}_m)$$
$$\times\hat{\zeta}(k_1,\omega_1)\cdots\hat{\zeta}(k_m,\omega_m)\delta(\vec{k}_1+\vec{k}_2+\cdots+\vec{k}_m-\vec{k})$$
$$\times\delta(\omega-\omega_1-\omega_2-\cdots-\omega_m)(2\pi)^3 . \tag{3.7a}$$

The coefficients $W^{(m)}$ are symmetric under interchange of the indices $2,3,\ldots,m$, and explicit expressions for $W^{(2)}$ and $W^{(3)}$ are listed in Appendix A. The ω dependence in expression (3.7) reflects the implicit dependence of $\zeta(x,t)$ on time, where

$$\hat{\zeta}(k,\omega)=\int dx\int dt\, e^{-ikx-i\omega t}\zeta(x,t) . \tag{3.7b}$$

The reason for the inclusion of the dependence of $\hat{w}(k,\omega)$ on ω will become clear when we consider the full equation of motion for $\zeta(x,t)$.

We next turn our attention to the equation for the solute field. The relevant Green's function is (for details see II)

$$G(p\mid p_1)=\frac{1}{(4\pi\tau)^{3/2}}\exp\frac{-\Delta^2}{4\tau} , \tag{3.8}$$

which satisfies the following equation:

$$\left[\nabla_1^2-2\frac{\partial}{\partial z_1}+\frac{\partial}{\partial t_1}\right]G(p\mid p_1)=-\delta(p-p_1) , \tag{3.9}$$

where p denotes the space-time point $(\vec{x},z,t)$ and $\tau=t-t_1$. The quantity Δ^2 in expression (3.8) is of the form

$$\Delta^2=(\vec{x}-\vec{x}_1)^2+[(z-z_1)+2\tau]^2 , \tag{3.10}$$

and $\vec{x}$ is a two-dimensional vector perpendicular to the z axis.

Multiplying Eq. (3.9) by $u(p_1)$ and integrating over time and space, we find

$$u(p)=\int_{-\infty}^{t}dt_1\int_{v_L}dv_1\left[-\frac{\partial}{\partial t_1}+2\frac{\partial}{\partial z_1}\right]u(p_1)G(p\mid p_1)$$
$$-\int_{-\infty}^{t}dt_1\int_{S_L}dS_1[G(p\mid p_1)\vec{\nabla}_1u(p_1)-u(p_1)\vec{\nabla}_1G(p\mid p_1)]\cdot\vec{n} . \tag{3.11}$$

The first term in the first integral above gives no contribution. As before, we let the outer part of the surface S_L go to infinity and the bottom part approach the interface. If we also make use of the boundary condition (2.10), we have

$$u(p)=2\int dt_1\int d^2x_1G(p\mid p_1^{\rm int})[1-u(p_1^{\rm int})]$$
$$+\int dt_1\int d^2x_1G(p\mid p_1^{\rm int})\left[2+\frac{d\zeta_1}{dt_1}\right][\kappa+(1-\kappa)u(p_1^{\rm int})]$$
$$+\int dt_1\int_{S_L}dS_1[u(p_1^{\rm int})-1]\vec{\nabla}_1G(p\mid p_1^{\rm int})\cdot\hat{n} , \tag{3.12}$$

where we have used the following identity[10]:

$$\int dt_1 \int_{S_L} dS_1 \, \vec{\nabla}_1 G(p \mid p_1)\cdot\hat{n} = \int dt_1 \int d^2x_1 \hat{z}\cdot\vec{\nabla}_1 G(\vec{x},z,t \mid \vec{x}_1,z_S,t_1) = e^{-2(z-z_S)} . \tag{3.13}$$

The notation in the above equation is indicated in Fig. 3. We now let the point $\vec{r}$ approach the interface. The term containing $\vec{\nabla}_1 G$ in Eq. (3.12) is singular for $\vec{r}\to\vec{r}_{\rm int}$; however, this is an integrable singularity and its contribution can be easily evaluated as shown in Appendix B. The final result is

$$1+u(p^{\rm int})-\int_{-\infty}^{t} dt_1 \int d^2x_1 G(p^{\rm int} \mid p_1^{\rm int}) \left\{ \frac{(\Delta\zeta-\vec{\nabla}_1\zeta_1\cdot\Delta\vec{x})}{\tau}[u(p_1^{\rm int})-1] + 2\frac{d\zeta_1}{dt_1}[\kappa+(1-\kappa)u(p_{\rm int})]+2[1+2\kappa+(1-2\kappa)u(p_1^{\rm int})] \right\} = 0 . \tag{3.14}$$

Equation (3.14), together with the expression (3.7), is the basic integro-differential equation upon which all of our analysis is based.

IV. EXPANSION SCHEME AND LINEAR STABILITY ANALYSIS

Other than using direct numerical techniques, it is difficult to find even approximate stationary solutions of Eq. (3.14). An expansion scheme, however, will enable us to investigate states which are small in amplitude. The strategy, therefore, will be to expand (3.14) in powers of ζ but to keep only a finite number of terms in the hope of finding some approximate solutions. Following II, we write Eq. (3.14) in the form

$$\sum_{n=1}^{\infty} \mathscr{B}^{(n)}(\vec{x},t,\{\zeta\}) = 0 , \tag{4.1}$$

where the $\mathscr{B}^{(n)}$'s are nth-order integro-differential operators on $\{\zeta\}$. Taking the Fourier transform of expression (4.1), we obtain expressions for the individual terms

$$\hat{\mathscr{B}}^{(n)}(\vec{k},\omega,\{\zeta\}) = \int \frac{d^2k_1}{(2\pi)^2}\cdots\int\frac{d^2k_n}{(2\pi)^2}\int\frac{d\omega_1}{2\pi}\cdots\int\frac{d\omega_n}{2\pi} B^{(n)}(\vec{k},\omega \mid \vec{k}_1,\omega_1,\vec{k}_2,\omega_2,\ldots,\vec{k}_n,\omega_n)\,\hat{\zeta}(k_1,\omega_1)\cdots\hat{\zeta}(k_n,\omega_n) \times(2\pi)^3\delta(\vec{k}_1+\vec{k}_2+\cdots+\vec{k}_n-\vec{k})\,\delta(\omega_1+\omega_2+\cdots+\omega_n-\omega) . \tag{4.2}$$

In evaluating the $B^{(n)}$, we must use the coefficients $W^{(n)}$ already obtained from the expansion for $u_{\rm int}$, i.e., the expansion (3.7). The normalization of the $B^{(n)}$'s is chosen as specified by the form in which Eq. (3.14) is written. Explicit expressions for

$$B^{(1)}(\vec{k},\omega \mid \vec{k},\omega) ,$$

$$B^{(2)}(\vec{k},\omega \mid \vec{k}_1,\omega_1,\vec{k}_2,\omega_2) ,$$

and

$$B^{(3)}(\vec{k},\omega \mid \vec{k}_1,\omega_1,\vec{k}_2,\omega_2,\vec{k}_3,\omega_3)$$

are given in Appendix C.

A trivial solution of Eq. (4.1) is

$$\zeta(x,t)=0 . \tag{4.3}$$

This solution corresponds to the flat or planar interface. To investigate the stability of this solution we need only consider the leading term in the sum (4.1). In Fourier space,

$$B^{(1)}(\vec{k},\tilde{\omega} \mid \vec{k},\tilde{\omega})\hat{\zeta}(\vec{k},\tilde{\omega}) = 0 , \tag{4.4}$$

where

$$B^{(1)}(\vec{k},\omega \mid \vec{k},\omega) = 2-1/\bar{v}-\xi k^2 - \frac{1}{h}[2-E(1/\bar{v}+\xi k^2)+i\omega] . \tag{4.5}$$

Here

$$E = 1-2\kappa \tag{4.6a}$$

and

$$h = (1+k^2+i\omega)^{1/2} . \tag{4.6b}$$

Solving for $i\tilde{\omega}(\vec{k})$, we get

$$i\tilde{\omega}(\vec{k}) \equiv \Omega(\vec{k}) = x_1 + \tfrac{1}{2}x_2^2 + x_2(1+k^2+x_1+\tfrac{1}{4}x_2^2)^{1/2} , \tag{4.7}$$

where

$$x_1 = -2 + E(1/\bar{v} + \xi k^2)$$

and (4.8)

$$x_2 = 2 - 1/\bar{v} - \xi k^2 .$$

A plot of $\Omega(\vec{k})$ vs $\vec{k}$ for fixed ξ and E is shown in Fig. 4 for several values of $\bar{v}$. We see that there is a critical value of $\bar{v}$ below which the planar interface is differentially stable against all infinitesimal perturbations. As $\bar{v}$ is increased beyond $\bar{v}_c$, a band of unstable modes appears which widens rapidly as $\bar{v}$ is increased. The critical point is determined by the condition that the maximum of $\Omega(\vec{k})$ pass through a zero. For a given value of E and ξ, the critical parameters $\bar{v}_c$ and k_c are related as follows:

$$\frac{1}{\nu_c \xi} = \frac{2h_{0c}(h_{0c}-1)(h_{0c}-E) - k_c^2(1-E)}{1-E} \tag{4.9a}$$

and

$$\frac{1}{\xi} = \frac{h_{0c}(h_{0c}-E)^2}{1-E} , \tag{4.9b}$$

where

$$h_{0c} = (1+k_c^2)^{1/2} . \tag{4.9c}$$

Equations (4.9) imply that there exists a value of $\xi = \xi^*$ such that for

$$\xi \to \xi^* = \frac{1}{(1-E)} , \quad k_c \to 0 \text{ and } 1/\bar{v}_c \to 0 . \tag{4.10}$$

A plot of $\bar{v}_c(\xi)$ for $E=0$ is shown in Fig. 6 where $\bar{v}_c(\xi)$ is denoted by the dotted line. The planar interface is stable at values of $\bar{v}$ and ξ which lie below the dotted line. In the region above the curve $\bar{v}_c(\xi)$, the planar interface is unstable and there exists a band of wave numbers with positive amplification rate $[\Omega(\vec{k}) > 0]$. The width of this band is directly related to the distance of the system from the marginal stability curve $\bar{v}_c(\xi)$. If we denote by $[k_1, k_2]$ the band of unstable wave numbers, where k_1 and k_2 are the zeros of the amplification rate, then for $\bar{v}$ only slightly larger than $\bar{v}_c$, we note that $\Omega(\vec{k})$ for $k_1 < |\vec{k}| < k_2$ is small. Therefore we can expand (4.5) in $i\omega$ to obtain the following expression for $\Omega(\vec{k})$ to lowest order:

$$\Omega(\vec{k}) = \frac{iB^{(1)}(\vec{k},0 \mid \vec{k},0)}{\left.\dfrac{\partial B^{(1)}}{\partial \omega}\right|_{\omega=0}} . \tag{4.11}$$

This expression for $\Omega(\vec{k})$ agrees with (4.7) to 0.1% for $k_1 < |k| < k_2$ and the values of $\bar{v}$ shown in Fig. 4. Equation (4.11) will prove to be useful in the following analysis.

V. STATIONARY STATES

In this section we will look for stationary solutions of Eq. (4.1). We will consider a two-dimensional geometry so that $\zeta = \zeta(x,t)$. Therefore, the following analysis will only apply to thin-film samples. We will limit our attention to values of $\bar{v}$ for which the amplitude of the nonzero stationary states (if they exist) is small. This will ensure that our truncation scheme (4.1) is valid.

The details of the stability analysis presented in Sec. IV lead us to assume that if $\bar{v} \gtrsim \bar{v}_c$, stationary solutions will have fundamental periodicities $2\pi/k_0$, where k_0 is a wave number in the range $k_1 < k_0 < k_2$ where $\Omega(\vec{k})$ is small and positive. We will further assume that the dynamical behavior of the system will be determined by the behavior of these slow modes $[\Omega(\vec{k}_0) \ll 1]$.

We will look for stationary solutions of the form

$$\zeta(x, t=0) = \sum_n A_n e^{ink_0 x} . \tag{5.1}$$

We would also like to develop a means to investigate the stability of such solutions against perturbations

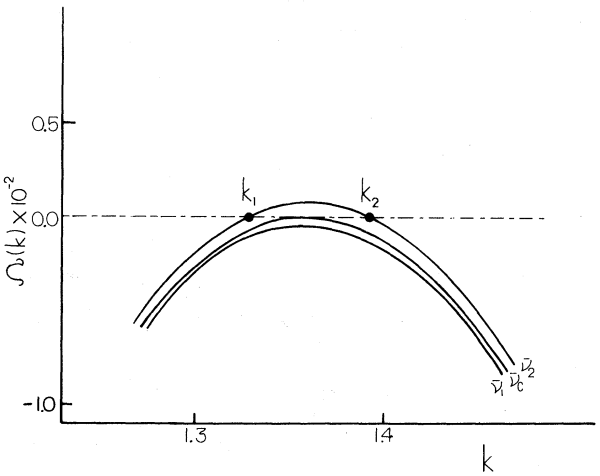

FIG. 4. Plot of $\Omega(k)$ for $E=0.6$, $\beta=1$, and $\xi=0.2$ at three different values of $\bar{v}$, where $\bar{v}_1 = 1.117\,25$, $\bar{v}_c = 1.117\,52$, and $\bar{v}_2 = 1.118\,25$.

which are small but which destroy the perfect long-range periodicity. To describe these small dynamical excursions away from the stationary state (5.1), we will allow the amplitudes A_n to be functions of x and t with the understanding that such dependence is weak. Thus we will consider an ansatz for $\zeta(x,t)$ of the form

$$\zeta(x,t)=\sum_n A_n(x,t)e^{ink_0x} . \tag{5.2}$$

We will assume that all the amplitudes A_n depend weakly on t for the following reason: We saw that for $k_1<k_0<k_2$, $\Omega(k_0)$ is small; hence we expect $A_1(x,t)$ to evolve slowly as a function of time. However, $\Omega(n\vec{k}_0)$ for $n=2,3,\ldots,$ is negative and large for $\bar{v}\gtrsim\bar{v}_c$; therefore, we expect these modes to relax quickly to strengths determined by the instantaneous value of A_1. Thus, apart from initial transients, the amplitudes $A_2,A_3,\ldots,$ will be weak functions of time. The assumption of weak dependence of the amplitudes on x implies that deviations from perfect spatial periodicity occur slowly, over distances much larger than the fundamental wavelength $2\pi/k_0$. Our method will break down for stronger spatial variations.

The truncated equation of motion in Fourier space is

$$\sum_{n=1}^{3}\hat{\mathscr{B}}^{(n)}(k,\omega,\{\hat{\zeta}\})=0 , \tag{5.3}$$

where the $\hat{\mathscr{B}}^{(n)}$ are as in Eq. (4.2). Taking the Fourier transform of the ansatz (5.2) for $\zeta(x,t)$, we obtain

$$\hat{\zeta}(k,\omega)=\int dx\int dt\, e^{-ikx-i\omega t}\times\sum_m A_m(x,t)e^{imk_0x} , \tag{5.4}$$

where

$$A_{-m}(x,t)=A_m^*(x,t) , \tag{5.5}$$

where the asterisk denotes complex conjugation. With the following change of variable:

$$\Delta k_m=k-mk_0 , \tag{5.6}$$

we can rewrite (5.3) in a form which is convenient for both the steady-state and stability analyses.

Consider in particular the term $\mathscr{B}^{(2)}$,

$$\hat{\mathscr{B}}^{(2)}(k,\omega,\{\hat{\zeta}\})=\sum_p\sum_q\int\frac{d\Delta k_p}{2\pi}\int\frac{d\Delta k_q}{2\pi}\int\frac{d\omega_p}{2\pi}\int\frac{d\omega_q}{2\pi}B^{(2)}(k,\omega\,|\,pk_0+\Delta k_p,\omega_p,qk_0+\Delta k_q,\omega_q)(2\pi)^2\times\hat{\zeta}(\Delta k_p,\omega_p)\hat{\zeta}(\Delta k_q,\omega_q)\delta(pk_0+\Delta k_p+qk_0+\Delta k_q-k)\times\delta(\omega_p+\omega_q-\omega) , \tag{5.7}$$

where

$$\hat{\zeta}(\Delta k_p,\omega_p)=\int dx\int dt\, e^{i(\Delta k_p x+\omega_p t)}A_p(x,t) . \tag{5.8}$$

Taking the inverse Fourier transform of (5.7), we find

$$\mathscr{B}^{(2)}(x,t,\{\zeta\})=\sum_p\sum_q\int\frac{d\Delta k_p}{2\pi}\int\frac{d\Delta k_q}{2\pi}\int\frac{d\omega_p}{2\pi}\int\frac{d\omega_q}{2\pi}\hat{B}^{(2)}(k,\omega\,|\,pk_0+\Delta k_p,\omega_p,qk_0+\Delta k_q,\omega_q)e^{ipk_0x}\times e^{iqk_0x}\hat{\zeta}(\Delta k_p,\omega_p)\hat{\zeta}(\Delta k_q,\omega_q)e^{i\Delta k_p x+i\omega_p t}e^{i\Delta k_q x+i\omega_q t} , \tag{5.9}$$

where

$$k=pk_0+\Delta k_p+qk_0+\Delta k_q \tag{5.10a}$$

and

$$\omega=\omega_p+\omega_q . \tag{5.10b}$$

We can now expand the function $B^{(2)}$ in powers of Δk_m and ω_m to obtain the following expression:

$$\begin{aligned}\mathscr{B}^{(2)}(x,t,\{\zeta\})=&\sum_p\sum_q A_p(x,t)e^{ipk_0x}A_q(x,t)e^{iqk_0x}B_0^{(2)}(nk_0\,|\,pk_0,qk_0)\\&+\sum_p\sum_q A_p(x,t)\frac{\partial A_q(x,t)}{\partial x}e^{i(p+q)k_0x}\frac{\partial B^{(2)}}{\partial k_q}\bigg|_{\omega=0,\ \Delta k=0}+\begin{bmatrix}p\to q\\ q\to p\end{bmatrix}\\&+\sum_p\sum_q A_p(x,t)\frac{\partial A_q(x,t)}{\partial t}e^{i(p+q)k_0x}\frac{\partial B^{(2)}}{\partial\omega_q}\bigg|_{\omega=0,\ \Delta k=0}+\begin{bmatrix}p\to q\\ q\to p\end{bmatrix}+O((\Delta k)^2)+O(\omega^2) ,\end{aligned} \tag{5.11}$$

where

$$n=p+q \ .$$

We have also introduced the following notation:

$$B_0^{(N)}(k \mid k_1,k_2,\ldots,k_n)\equiv B^{(n)}(k,\omega=0 \mid k_1,\omega_1=0,\ldots,k_n,\omega_n=0) \ .$$

Expressions similar to (5.11) can be obtained for $\mathscr{B}^{(1)}(x,t,\{\zeta\})$ and $\mathscr{B}^{(3)}(x,t,\{\zeta\})$. We finally obtain a system of coupled differential equations for the amplitudes $A_m(x,t)$.

In order to look for stationary states of the form (5.1), we set ω_m and Δk_m equal to zero in expression (5.3). We then obtain for $n=0,1,2,3,\ldots,$ the following system of equations:

For $n=0$,

$$B_0^{(1)}(0 \mid 0)A_0+2B_0^{(2)}(0 \mid k_0,-k_0)A_1A_1+2B_0^{(2)}(0 \mid 2k_0,-2k_0)A_2A_2^*+\cdots=0 \ , \tag{5.12a}$$

for $n=1$,

$$B_0^{(1)}(k_0 \mid k_0)A_1+2B_0^{(2)}(k_0 \mid k_0,0)A_0A_1+2B_0^{(2)}(k_0 \mid 2k_0,-k_0)A_2A_1^*+2B_0^{(2)}(k_0 \mid 3k_0,-2k_0)A_2^*A_3$$
$$+3B_0^{(3)}(k_0 \mid k_0,k_0,-k_0)A_1^2A_1^*+\cdots=0 \ , \tag{5.12b}$$

for $n=2$,

$$B^{(1)}(2k_0 \mid 2k_0)A_2+B^{(2)}(2k_0 \mid k_0,k_0)A_1^2+2B^{(2)}(2k_0 \mid 2k_0,0)A_0A_2+2B^{(2)}(2k_0 \mid 3k_0,-k_0)A_1^*A_3$$
$$+3B^{(3)}(2k_0 \mid k_0,k_0,0)A_0A_1^2+6B^{(3)}(2k_0 \mid 2k_0,k_0,-k_0)A_1A_1^*A_2+\cdots=0 \ , \tag{5.12c}$$

for $n=3$,

$$B^{(1)}(3k_0 \mid 3k_0)A_3+2B^{(2)}(3k_0 \mid k_0,2k_0)A_1A_2+2B^{(2)}(3k_0 \mid 3k_0,0)A_0A_3$$
$$+B^{(3)}(3k_0 \mid k_0,k_0,k_0)A_1^3+\cdots=0 \ , \tag{5.12d}$$

and so on for $n=4,5,\ldots,$.

We wish to find a solution of these equations consistent with the fact that for $\bar{\nu}\geq\bar{\nu}_c$, the amplitude A_1 of the fundamental is dominant but small. Thus if A_1 is small, Eqs. (5.12) imply that $A_0\propto A_1^2$, $A_2\propto A_1^2$, $A_3\propto A_1^3$, etc., and in general $A_n\propto A_1^n$. If we keep terms of order A_1^3 in these equations, we obtain the following results:

$$A_0=-2\frac{B_0^{(2)}(0 \mid k_0,-k_0)}{B_0^{(1)}(0 \mid 0)}A_1A_1^*+O(A_1^3) \ , \tag{5.13}$$

$$A_2=-\frac{B_0^{(2)}(2k_0 \mid k_0,k_0)}{B_0^{(1)}(2k_0 \mid 2k_0)}A_1^2+O(A_1^3) \ . \tag{5.14}$$

A nontrivial solution for A_1 exists of the form

$$A_1^2=A_1A_1^*=\frac{B_0^{(1)}(k_0 \mid k_0)}{a_1} \ , \tag{5.15}$$

where

$$a_1=4\frac{B_0^{(2)}(0 \mid k_0,-k_0)}{B_0^{(1)}(0 \mid 0)}B^{(2)}(k_0 \mid k_0,0)$$
$$+2\frac{B^{(2)}(2k_0 \mid k_0,k_0)}{B^{(1)}(2k_0 \mid 2k_0)}B^{(2)}(k_0 \mid 2k_0,-k_0)-3B_0^{(3)}(k_0 \mid k_0,k_0,-k_0) \ . \tag{5.16}$$

Here we have used Eqs. (5.13) and (5.14) to eliminate A_0 and A_2 from Eq. (5.12b). We see that A_1 is coupled to A_0 (the average position of the interface), and more importantly to A_2, the amplitude of the first harmonic. We see from (5.15) that $A_1\sim\sqrt{\Delta\nu}$ where $\Delta\nu=\bar{\nu}-\bar{\nu}_c$.

For k_0 in the domain $[k_1,k_2]$, $B_0^{(1)}(k_0 \mid k_0)$ is positive, so that a solution exists for values of the coefficient a_1 which are positive. We can use Eq. (5.15) to determine the regions of parameter space where states of the form (5.13) and (5.15) exist. From now on we will term this solution the "one-mode solution," because only one mode is dominant. To find the region of parameter space in which the solution (5.15) exists and is valid, we will monitor the sign of a_1 at the critical point: $\bar{\nu}=\bar{\nu}_c$ and $k_0=k_c$. There exists a value of $\xi=\xi_c$ such that $a_1=0$ at the critical point.

The remaining independent parameters are E and β. In Fig. 5 we show the value of k_c at which a_1 changes sign as a function of E for values of β equal to 1 and 2. In the regions below the curves, a_1 is positive, and a one-mode solution exists with vanishingly small amplitude at the onset of instability. Note that for $\beta=1$, the curve diverges at $E\cong 0.1$, so that solutions with arbitrarily large wave vectors can be obtained by an appropriate choice of the remaining system parameters. We will discuss this point further in Sec. VII, where we consider this fact with respect to real systems. The curve for $\beta=2$ always stays finite, which puts a general upper bound on the wave number of a one-mode solution. The results for $\beta=2$ agree with those obtained by Wollkind and Segel.[4]

As $\bar{\nu}$ is increased, the band $[k_1,k_2]$ grows, and eventually must become wide enough for both a fundamental k_0 and a first-harmonic $2k_0$ to be simultaneously unstable. However, long before we reach this situation, we must expect that higher-order couplings will become important and must be included. For example, we expect a coupling of the form $A_1^2A_2$ to be important. To choose the next most important terms in Eqs. (5.12), we will assume that both A_1 and A_2 are of the same order of magnitude, i.e., $A_1\sim A_2\sim\sqrt{\Delta\nu}$. Therefore A_3 and A_4 are to lowest order given by

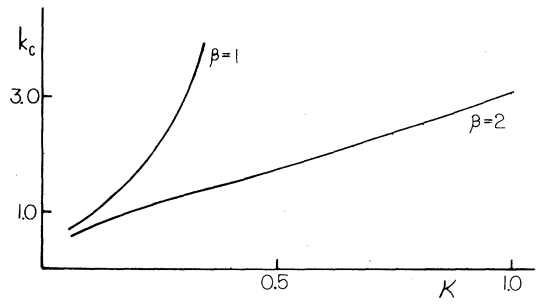

FIG. 5. We show the value of k_c at which the coefficient a_1 is zero as a function of the partition coefficient κ for β equal to 1 and 2.

$$A_3=-2\frac{B_0^{(2)}(3k_0 \mid 2k_0,k_0)}{B_0^{(1)}(3k_0 \mid 3k_0)}A_1A_2+O(A^3)\,, \tag{5.17}$$

$$A_4=-\frac{B_0^{(2)}(4k_0 \mid 2k_0,2k_0)}{B_0^{(1)}(4k_0 \mid 4k_00)}A_2^2+O(A^3)\,, \tag{5.18}$$

and

$$A_0=\frac{-2}{B_0^{(1)}(0 \mid 0)}[B_0^{(2)}(0 \mid k_0,-k_0)A_1^2+B_0^{(2)}(0 \mid 2k_0,-2k_0)A_2^2]+O(A^3)\,. \tag{5.19}$$

If we now use Eqs. (5.17)–(5.19) to substitute for A_3, A_4, and A_0 in Eqs. (5.12b) and (5.12c), we get the following coupled equations:

$$B_0^{(1)}(k_0 \mid k_0)A_1+2B_0^{(2)}(k_0 \mid 2k_0,-k_0)A_1^*A_2+\alpha_1(k_0)A_1A_2A_2^*+\alpha_2(k_0)A_1^2A_1^*=0\,, \tag{5.20}$$

$$B_0^{(2)}(2k_0 \mid 2k_0)A_2+B_0^{(2)}(2k_0 \mid k_0,k_0)A_1^2+\beta_1(k_0)A_1A_1^*A_2+\beta_2(k_0)A_2^2A_2^*=0\,, \tag{5.21}$$

where

$$\alpha_1(k_0)=-4\frac{B_0^{(2)}(0 \mid 2k_0,-2k_0)}{B_0^{(1)}(0 \mid 0)}B_0^{(2)}(k_0 \mid k_0,0)+6B_0^{(3)}(k_0 \mid 2k_0,-2k_0,k_0)$$

$$-4\frac{B_0^{(2)}(3k_0 \mid 2k_0,k_0)}{B_0^{(1)}(3k_0 \mid 3k_0)}B_0^{(2)}(k_0 \mid 3k_0,-2k_0)\,, \tag{5.22}$$

$$\alpha_2(k_0)=3B_0^{(3)}(k_0 \mid k_0,k_0,-k_0)-4\frac{B_0^{(2)}(0 \mid k_0,-k_0)}{B_0^{(1)}(0 \mid 0)}B_0^{(2)}(k_0 \mid k_0,0)\,, \tag{5.23}$$

$$\beta_1(k_0)=6B_0^{(3)}(2k_0\,|\,2k_0,k_0,-k_0)-4\frac{B_0^{(2)}(0\,|\,k_0,-k_0)}{B_0^{(1)}(0\,|\,0)}B_0^{(2)}(2k_0\,|\,2k_0,0)$$
$$-4\frac{B_0^{(2)}(3k_0\,|\,2k_0,k_0)}{B_0^{(1)}(3k_0\,|\,3k_0)}B_0^{(2)}(2k_0\,|\,3k_0,-k_0)\,, \tag{5.24}$$

and

$$\beta_2(k_0)=3B_0^{(3)}(2k_0\,|\,2k_0,2k_0,-2k_0)-2\frac{B_0^{(2)}(4k_0\,|\,2k_0,2k_0)}{B_0^{(1)}(4k_0\,|\,4k_0)}B_0^{(2)}(2k_0\,|\,4k_0,-2k_0)$$
$$-4\frac{B_0^{(2)}(0\,|\,2k_0,-2k_0)}{B_0^{(1)}(0\,|\,0)}B_0^{(2)}(2k_0\,|\,2k_0,0)\,. \tag{5.25}$$

We must note here that we can only expect Eqs. (5.20) and (5.21) to give approximate solutions in regions of parameter space where the assumptions made in their derivation are valid, that is, the amplitudes are small. We must also check the coefficients of the above terms to see that they are "well behaved" in the domain of k, within which we are looking for solutions. By well behaved we mean that they do not have zeros or diverge for some values of k, ξ, ν, E, and β. The results presented in Sec. VII are in regions of the parameter space (k, ξ, ν, E, and $\beta=1$), where our assumptions are valid and we monitor both the coefficients and the sizes of the various couplings for A_1 and A_2. We will call Eqs. (5.20) and (5.21) the "two-mode equations."

From Eq. (5.20) we can solve for $A_1A_1^*$ to get

$$A_1A_1^*=A_1^2=\frac{1}{\alpha_2}[B_0^{(1)}(k_0\,|\,k_0)$$
$$+2B_0^{(2)}(k_0\,|\,2k_0,-k_0)A_2$$
$$+\alpha_1A_2A_2^*]\,. \tag{5.26}$$

On substituting this expression for A_1^2 into Eq. (5.21), we obtain a cubic equation for A_2 which we can solve for real solutions. There exists at least one, and at most three, real solutions for A_2, depending on the behavior of the coefficients of the resulting cubic equation for A_2. On substituting these solutions back into (5.26) we may or may not obtain a real value for A_1.

VI. ONE-MODE AND TWO-MODE STABILITY ANALYSES

We now turn our attention to the stability of the stationary states described in the preceding section. We will consider the expansion of the truncated equation (5.3) in powers of Δk and ω as illustrated by Eq. (5.11). We will keep only the lowest-order terms in ω and will consider deviations Δk away from the stationary state at fundamental wave number k_0 such that Δk is small and of order $A_1(k_0)$. Collecting terms up to order A_1^3, we obtain the following equation:

$$\alpha_3\frac{\partial}{\partial t}A_1(x,t)+\alpha_4\frac{\partial}{\partial x}A_1(x,t)+\alpha_5\frac{\partial^2}{\partial x^2}A_1(x,t)$$
$$+B_0^{(1)}(k_0\,|\,k_0)A_1(x,t)-a_1A_1^*(x,t)A_1^2(x,t)=0\,, \tag{6.1}$$

where

$$\alpha_3=i\frac{\partial B^{(1)}(k,\omega\,|\,k,\omega)}{\partial\omega}\bigg|_{\omega=0,\ \Delta k=0,\ k=k_0,}\,, \tag{6.2a}$$

$$\alpha_4=i\frac{\partial B^{(1)}(k,\omega\,|\,k,\omega)}{\partial k}\bigg|_{\omega=0,\ k=k_0,\ \Delta k=0}\,, \tag{6.2b}$$

and

$$\alpha_5=-\frac{1}{2}\frac{\partial^2B^{(1)}(k,\omega\,|\,k,\omega)}{\partial k^2}\bigg|_{\omega=0,\ k=k_0,\ \Delta k=0}\,. \tag{6.2c}$$

Using Eq. (6.1) we can investigate the stability of a state at wave number k_0 against perturbations which disturb the long-range periodicity of the state. However, before we proceed to this analysis, we should mention some of the properties of Eq. (6.1).

First, if there is another stationary state close to k_0, at k_0' for instance, then as long as $|k_0-k_0'|$ is small of the order of $\sqrt{\Delta\nu}$, we can expect to find the state at k_0' as a solution of Eq. (6.1). Clearly there is a special situation for $\bar{\nu}\gtrsim\nu_c$ such that $\bar{\nu}-\bar{\nu}_c=\Delta\nu$ is small and $|k_1-k_2|$ is of order $\sqrt{\Delta\nu}$. In this case the coefficient α_4 is small and can be neglected; the resulting equation describes the dynamic behavior of the unstable band of wave numbers $[k_1,k_2]$ about k_c. Such an equation is analogous to the amplitude

equation derived by Newell and Whitehead[11] to describe the dynamics near the onset of convection in a fluid. A more rigorous derivation of the amplitude equation for the solidification model is presented elsewhere, and the equation is used to simulate the dynamical behavior of the system for $\bar{v}\approx\bar{v}_c$.[12] However, if we are interested only in questions of stability, Eq. (6.1) will provide the information necessary for such a determination.

In the two-mode approximation, we will follow a procedure similar to that outlined above. We assume that $\Delta k\sim A_1\sim A_2\sim\sqrt{\Delta v}$. We will again keep only lowest-order terms in ω. The resulting equations are

$$\alpha_3\frac{\partial}{\partial t}A_1+\alpha_4\frac{\partial}{\partial x}A_1+\alpha_5\frac{\partial^2 A_1}{\partial x^2}+\alpha_6 A_1^*\frac{\partial}{\partial x}A_2+\alpha_7 A_2\frac{\partial}{\partial x}A_1^*+B^{(1)}(k_0\mid k_0)A_1+2B^{(2)}(k_0\mid 2k_0,-k_0)A_1^*A_2$$
$$+\alpha_1(k_0)A_1A_2A_2^*+\alpha_2(k_0)A_1^2A_1^* \quad (6.3a)$$

and

$$\beta_3\frac{\partial}{\partial t}A_2+\beta_4\frac{\partial}{\partial x}A_2+\beta_5\frac{\partial^2}{\partial x^2}A_2+\beta_6 A_1\frac{\partial}{\partial x}A_1+B^{(1)}(2k_0\mid 2k_0)A_2+B^{(2)}(2k_0\mid k_0,k_0)A_1^2$$
$$+\beta_1(k_0)A_1A_1^*A_2+\beta_2(k_0)A_2^2A_2^*\ , \quad (6.3b)$$

where expressions for the coefficients α_3, α_4, α_5, α_6, α_7, β_3, β_4, β_5, and β_6 are given in Appendix D. Using these equations, we can determine the stability of the two-mode stationary solutions against perturbations which destroy the long-range periodicity of the solutions.

We will denote a stationary solution of the one-mode equation (5.15) by $A_{1s}(k_0)$. This will be a uniform solution of Eq. (6.1). We will perturb this solution in the following manner:

$$A_1(x,t)=A_{1s}(k_0)+\phi(x,t)\ . \quad (6.4)$$

If we now substitute this expression in Eq. (6.1) and linearize in the perturbation, we obtain the following equation for ϕ:

$$\alpha_3\partial_t\phi+\alpha_4\partial_x\phi+\alpha_5\partial_x^2\phi+B^{(1)}(k_0\mid k_0)\phi+2a_1(k_0)A_{1s}^2(k_0)\phi+a_1(k_0)A_{1s}^2(k_0)\phi^*(x,t)=0\ . \quad (6.5)$$

Solutions of this equation exist which are of the form

$$\phi=v_1(t)e^{i\delta_x x}+v_2(t)e^{-i\delta_x x}\ , \quad (6.6)$$

where v_1 and v_2 are both proportional to $e^{\lambda t}$. Substituting (6.6) in (6.5), we obtain from the condition for a solution to exist, a quadratic equation for λ. Solving for λ, we obtain the condition for a stable solution of the form (5.15), which is

$$\frac{d^2}{dk^2}\{[B_0^{(1)}(k\mid k)]^2\}\Big|_{k=k_0}<0\ . \quad (6.7)$$

Thus the stability of the stationary solution depends only on the function $B_0^{(1)}(k\mid k)$. For the two-mode solution, we will denote the stationary solution of Eqs. (5.20) and (5.21) by $A_{1s}(k_0),A_{2s}(k_0)$. We will consider perturbations of the form

$$A_1(x,t)=A_{1s}(k_0)+u_1(x,t)\ , \quad (6.8a)$$

$$A_2(x,t)=A_{2s}(k_0)+u_2(x,t)\ . \quad (6.8b)$$

As above, we substitute (6.8) in Eqs. (5.20) and (5.21) and linearize in u_1 and u_2. We obtain two coupled linear equations in u_1 and u_2, the details of which we will not present here. We then look for solutions of the form

$$u_1=\phi_1(t)e^{i\delta_x x}+\phi_2(t)e^{-i\delta_x x}\ , \quad (6.9a)$$

$$u_2=\phi_3(t)e^{i\delta_x x}+\phi_4(t)e^{-i\delta_x x}\ , \quad (6.9b)$$

where the functions $\phi_i(t)$ are all proportional to $e^{\lambda t}$. On substituting the solutions (6.9) into the linearized equations for u_1 and u_2, we obtain from the condition for a solution to exist, a quartic equation in λ. If we then solve for λ, the condition for the solution $[A_{1s}(k_0),A_{2s}(k_0)]$ to be stable is that all the solutions for λ have negative real parts.

VIII. REPRESENTATIVE ALLOY SYSTEM AND OUR RESULTS

In this section we will look for stable stationary solutions of the one- and two-mode equations as functions of the parameters E, β, ξ, k, and $\bar{v}$. To determine the domain of parameter space which is

relevant to real thin-film binary-alloy systems, we will first consider a representative fictitious system whose parameters are, to within an order of magnitude, equal to those of a real system.

A. Parameters

In our fictitious system we will set $T_m = 5\times 10^2$ K. Γ, which we define to be the ratio of the surface tension to the latent heat of fusion, is equal to 2×10^{-8} cm. The value of the slope of the liquidus m is equal to 2 K/wt. %. The solute diffusivity D in the liquid has the value 10^{-5} cm^2 sec^{-1}. We will consider systems whose phase diagrams are such that E lies in the domain $(-1,+1)$. In order to reduce the size of the parameter space, we will choose a value of $\beta=1$. In real systems, β ranges in value from 0.5 to 2. However, by a suitable choice of boundary conditions, we can restrict β to be close to 1. This can be simply accomplished by choosing the containing walls of the thin film to have a thermal conductivity much higher than the thermal conductivity of either the liquid or the solid phase of the alloy. The thermal gradient $\bar{G}$ imposed on the system can be used as a control parameter, but we should ensure that we choose values such that we do not develop convection currents in the liquid phase. However, one can suppress convection in the liquid in some systems by applying a weak magnetic field. In our fictitious system, we will fix $\bar{G}$ ($\bar{G}=G$ for $\beta=1$) at a value of 10 K/cm. The velocity v can also be used as a control parameter, but we must ensure that it is small so that our assumption that the interface is in thermal equilibrium is satisfied. Therefore we will consider velocities such that $0 \lesssim v \lesssim 10^{-2}$cm sec^{-1}. The concentration of solute C_0 can also be used as controlling parameter. We will consider values of this parameter in the domain $[10^{-3},1.0]$ wt. %.

Using definitions (2.1) through (2.5), we have that

$$\bar{v}=S_1 C_0 v \tag{7.1}$$

and

$$\xi=S_2\frac{v}{C_0}\ , \tag{7.2}$$

where

$$S_1=\frac{|m|(1+E)}{2\bar{G}D(1-E)}$$

and

$$S_2=\frac{T_m\Gamma(1-E)}{2D|m|(1+E)}\ .$$

By selecting a system with a phase diagram such that $E=0.0$, the constants S_1 and S_2 take on the following values:

$$S_1=10^4\ ,$$

measured in sec cm^{-1} (wt. %)$^{-1}$, and

$$S_2=0.25\ ,$$

measured in wt. % sec cm^{-1}.

Clearly, the values of the constants S_1 and S_2 may vary by an order of magnitude either way, depending on the system considered. However, with the above specifications for our representative system, it is clear that we should look for stationary states in the following domain of parameter space:

$$-1<E<1\ , \tag{7.3a}$$

$$0<\xi<1\ , \tag{7.3b}$$

$$\bar{v}\geq\bar{v}_c\ , \tag{7.3c}$$

and

$$\beta=1\ . \tag{7.3d}$$

We will map out regions of stable stationary states on plots of $\bar{v}$ vs ξ and $\bar{v}$ vs k. It will be useful, therefore, to see how the system point moves on such plots as a function of the control parameters v and C_0. In Fig. 6 we show a plot of $\bar{v}$ vs ξ showing

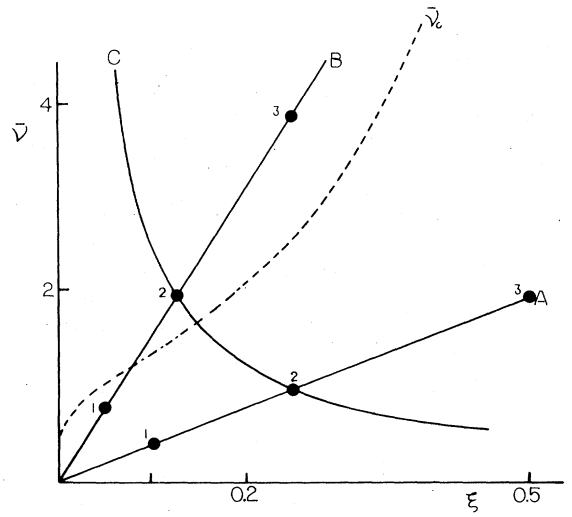

FIG. 6. Dotted line is a plot of $\bar{v}_c(\xi)$ for $E=0.0$ and $\beta=1$. In a system with $S_1=10^4$ sec cm^{-1} (wt. %)$^{-1}$ and $S_2=0.25$ wt. % sec cm^{-1}, the lines A and B correspond to the locus of points along which the system moves at $C_0=10^{-2}$ and 2×10^{-2} wt. %, respectively. The points labeled 1, 2, and 3 correspond to velocities of 4×10^{-3}, 10^{-2}, and 2×10^{-2} cm sec^{-1}, respectively. The curve C is the path along which the system moves on varying C_0 at fixed $V=2\times 10^{-2}$ cm sec^{-1} and fixed $\bar{G}$.

the curve (the dotted line) $\bar{v}_c(\xi)$ as computed for $E=0$ from (3.9a) and (3.9b). Also shown on this diagram are the lines A and B which correspond to the paths along which the system moves if one changes v at fixed C_0 and $\bar{G}$. The lines A and B correspond to values of C_0 equal to 10^{-2} and 2×10^{-2} wt.%, respectively. The points labeled 1, 2, and 3 correspond to velocities of 4×10^{-3}, 10^{-2}, and 2×10^{-2} cm sec^{-1}, respectively. The curve C in Fig. 6 corresponds to the system path if one changes C_0 at fixed v and $\bar{G}$. The particular curve shown corresponds to a value of v equal to 10^{-2} cm sec^{-1}. Finally, one can hold v and C_0 fixed and vary $\bar{G}$. In this case the system path would correspond to vertical lines in the ν-ξ plane.

From Fig. 6 we note that for a very dilute alloy, i.e., $C_0\sim10^{-2}$ wt.%, we cannot enter the unstable domain [above the dotted curve $\bar{v}_c(\xi)$] by increasing v. However, at higher solute concentrations, for instance, we can do so by moving along the line B. We note that for a special value of $C_0=\bar{C}_0$ (where $\bar{C}_0=1.665\sim10^{-2}$ wt.% for our fictitious system), the line along which the system moves by increasing v will be tangent to the curve $\bar{v}_c(\xi)$. For a system with a value of C_0 close to but greater than $\bar{C}_0$, we observe that by increasing the velocity, we will pass into the unstable domain at some critical value v_1, but by further increasing the velocity, we will return to the stable domain (i.e., to the domain where the planar interface is stable) at some velocity v_2. At values of C_0 of the order of 10^{-1} wt.% or higher, we will enter the unstable domain at values of $\bar{v}$ close to 0.5 ($\bar{v}=\nu$ for $\beta=1$, and $\nu<0.5$ corresponds to the supercooling criterion for stability of the planar interface), and we will remain in the domain of parameter space where ξ is very small, i.e., $\xi\ll0.1$ in our system. If we add small amounts of solute to the melt, we can vary C_0 and hence move the system along the curve C in Fig. 6, and the point where the planar interface becomes unstable can be chosen by a choice of a suitable value of v. Thus we see that by using v and C_0 we can effectively choose the value of k_c at which the planar interface becomes unstable.

B. Stable stationary states

We now present solutions of the one- and two-mode equations in the parameter space specified by (7.3). As a typical example of what is observed throughout regions of parameter space where states are observed, we consider the following example. For $E=-0.5$ and $\xi=0.01$, $\bar{v}_c=0.823\,349$ and $k_c=4.883\,97$. At $\bar{v}=0.823\,599$, we show, in Fig. 7, a plot of the amplitude $A_1(k)$ of the fundamental as a function of k. At this value of $\bar{v}$ the amplitudes

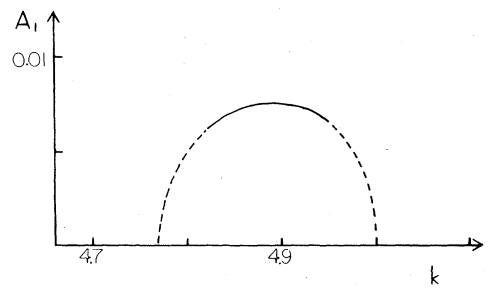

FIG. 7. Plot of the amplitude $A_1(k)$ as a function of k for $\bar{v}=0.823\,599$, $E=-0.5$, $\xi=0.01$, and $\beta=1$.

$A_1(k)$ and $A_2(k)$ as calculated from the one-mode and two-mode equations agree to a high degree of accuracy. The dotted line in Fig. 7 indicates that the state is unstable and the solid line indicates a stable state at that value of the wave number k. We only show the unstable solutions if they lie on the same solution branch as the stable solutions. A plot of the interface $\zeta_S(x)$ for $k=k_c$ is shown in Fig. 8. We note a slight back-front asymmetry but the fundamental is seen to dominate the solution with the higher harmonics making negligible contributions to the shape of the interface. As $\bar{v}$ is increased, the one- and two-mode solutions begin to show major discrepancies, particularly near values of k where the amplitude $A_1(k)$ has its maximum value. As $\bar{v}$ is increased, the higher-order couplings included in the two-mode approximation become important. Therefore we will use the two-mode equations to describe this domain of $\bar{v}$. On increasing $\bar{v}$, a gap develops in the domain $[k_1,k_2]$ and no stable solutions exist in this gap. As $\bar{v}$ is further increased, the gap widens and the stable branch of solutions lies on the lower-k branch of solutions as shown in Fig. 9 for $\bar{v}=0.834$. This stable band of solutions dimin-

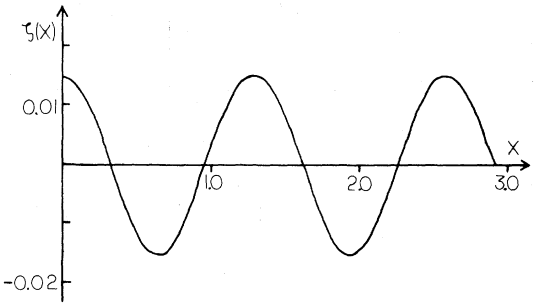

FIG. 8. Plot of the interface profile

$$\zeta(x)=\sum_{n=-4}^{4}A_n e^{inkx}$$

for $k=k_c$, $E=-0.5$, $\xi=0.01$, $\bar{v}=0.823\,599$, and $\beta=1$.

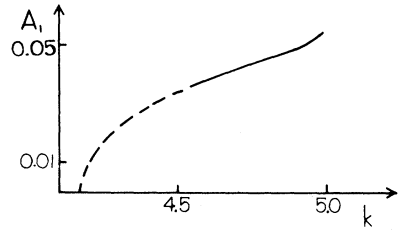

FIG. 9. Plot of the amplitude $A_1(k)$ as a function of k for $\bar{v}=0.834$, $E=-0.5$, $\xi=0.01$, and $\beta=1$. For this value of $\bar{v}$, $k_1=4.15794$ and $k_2=5.67122$.

ishes as $\bar{v}$ is increased and it vanishes at a value of $\bar{v}=\bar{v}_f(E,\xi)$. The interface at $k=4.8764$ and $\bar{v}=0.834$ is shown in Fig. 10. We note that the amplitude of the cellular interface has increased and that the front-back asymmetry has increased with the first harmonic playing a more important role.

The features described above are typical of what we observe in all domains of E, ξ, and ν where stable states are possible. Close to $\bar{v}_c$ we have a small band of stationary states over the entire range $[k_1,k_2]$ for which the planar interface is unstable. A smaller subset of these states are stable, the stable branch being centered on the state at k_c which is also close to the maximum amplitude state. As $\bar{v}$ is increased further, a gap develops in the domain of k for which stable solutions are possible. The stable branch of states shifts to lower values of k and the band of stable states narrows with increasing $\bar{v}$ until it vanishes at some value of $\bar{v}=\nu_f(E,\xi)$. The disappearance of this stable band is accompanied by an increased contribution to the interface profile by the first harmonic, and as a result the interface exhibits a front-back asymmetry with the leading portions of the interface becoming smoother and the trailing portions becoming sharper as shown in Fig. 10.

Having described the general behavior of the interface as $\bar{v}$ is increased, we now turn our attention to a systematic search of the parameter space. In Fig. 11 we show a plot of $\bar{v}$ vs k for $E=0.6$ and $\xi=0.2$. The dashed line is the neutral stability

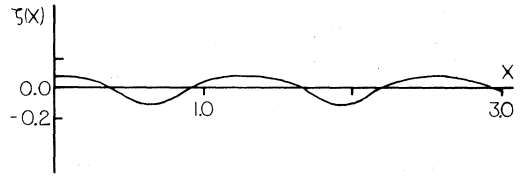

FIG. 10. Plot of the interface profile

$$\zeta(x)=\sum_{n=-4}^{4} A_n e^{inkx}$$

for $k=4.8764$, $\bar{v}=0.834$, $E=-0.5$, $\xi=0.01$, and $\beta=1$.

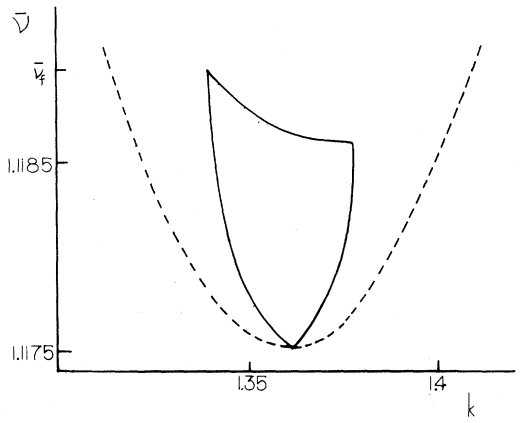

FIG. 11. Plot of $\bar{v}$ vs k showing the regions of stable stationary states (inside the solid curve) and the neutral stability curve (the dotted line) for $E=0.6$, $\xi=0.2$, and $\beta=1$.

curve and the region of stable stationary states lies inside the closed curve. We see that for $\bar{v}>\bar{v}_f=1.119$, no more stable solutions are possible.

In Fig. 12 we show a plot of $\bar{v}$ vs ξ showing the plots of $\bar{v}_f(E,\xi)$ and $\bar{v}_c(E,\xi)$ for $E=0.0$ and 0.6. The regions of stable stationary states (the shaded areas) are bounded above by $\bar{v}_f$ and below by $\bar{v}_c$. We observe that for a given value of E, $\delta\bar{v}\equiv(\bar{v}_f-\bar{v}_c)$ increases as a function of ξ for increasing ξ. A way of interpreting this fact is to say that as we increase the strength of the surface tension we increase the domain of $\bar{v}$ for which we can observe stationary stable states. In our example, where $\beta=1$, we note that for $E\geq 0.1$ there exists a

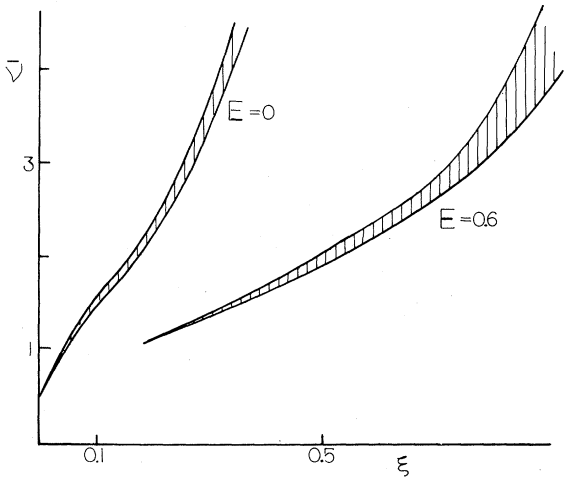

FIG. 12. Plot of $\bar{v}$ vs ξ showing the regions of stable cellular states for $E=0.0$ and 0.6. These regions are bounded above by $\bar{v}_f(\xi)$ and below by $\bar{v}_c(\xi,E)$.

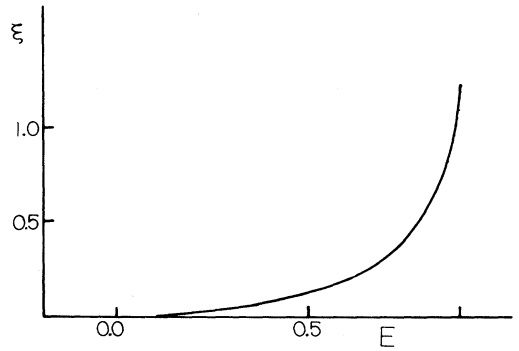

FIG. 13. Plot of ξ vs E where the region above the curve represents the domain of values of E and ξ for $\beta=1$, for which cellular states are possible.

value of $\xi=\bar{\xi}>0$ for which $\delta\bar{v}(\bar{\xi})=0$. A plot of $\bar{\xi}$ vs E is shown in Fig. 13. For $E<0.1$ and for $\beta=1$, it is therefore possible to observe stable states at $\bar{v}_c$ with wave vectors k_c which are arbitrarily large. However, we note that $\delta\bar{v}(\xi)$ is vanishingly small in this domain of ξ and hence we do not expect to be able to observe these states in experimental systems.

Having mapped out the domain of stable states for our system, we can now discuss a possible experiment. Let us again consider our fictitious alloy system whose parameters are given in Sec. VII A. We choose a system with a value of $E=0$. We will use the velocity v as our control parameter for the experiment and we will fix $G=10$ K/cm and $C_0=1.6749\times10^{-2}$ wt. %. The path the system will

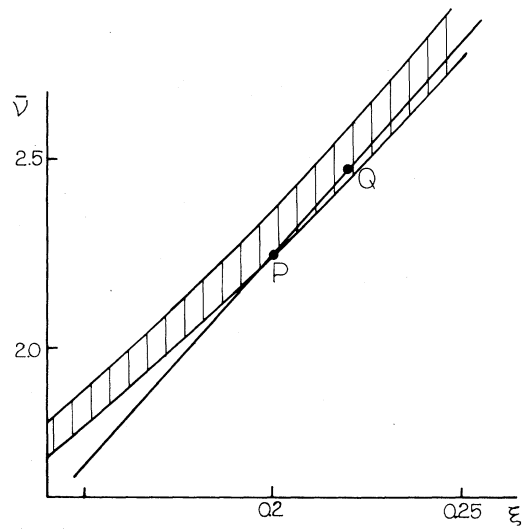

FIG. 14. Plot of $\bar{v}$ vs ξ showing the region of stable cellular states (the shaded region) and the path of the system (the line connecting the points P and Q) when the velocity v is charged.

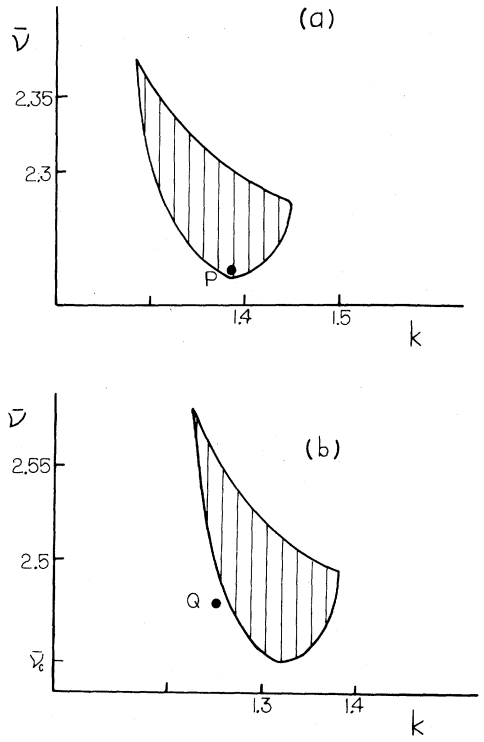

FIG. 15. Plot of $\bar{v}$ vs k for $E=0$, $\beta=1$, and (a) at a velocity v such that $\xi=0.2$; (b) at a velocity v such that $\xi=0.22$.

traverse in the $\bar{v}$-ξ plane is shown in Fig. 14 where the shaded region denotes the region of stable stationary states. As v is increased to a value $v_c=1.34\times10^{-2}$ cm sec^{-1} at the point P, the planar interface becomes unstable and a periodic pattern results with a characteristic fundamental wave vector close to $k=1.39$ as shown in Fig. 15(a). In unscaled units this corresponds to a cellular wavelength $\lambda_p=67.5$ μm. Thus since we are close to $\bar{v}_c$ we will observe an interface with a periodic structure which is strongly dominated by the fundamental wave vector. If we now increase the velocity by 10% we will move the system to the point labeled Q in Fig. 14. The corresponding stability diagram for this new value of the velocity is shown in Fig. 15(b). The periodic state with wavelength $\lambda=67.5$ μm is now at the point labeled Q in this figure and we see that it is outside the domain of allowed stable states. It will thus decay and be replaced by a new pattern in the domain of allowed stable states. The fundamental wave vector of the resulting pattern which is selected in the subsequent evolution is the topic of further research, but we conjecture that it will be close to the fastest growing mode at these new system parameters. This provides a mechanism for the

system to adjust its wavelength on increasing the velocity.

In the domain of parameter space where we find periodic states, we find that the amplitude of the state does not exceed a value which is about 20% of the wavelength of the periodic state. However, since the methods we have used to analyze the model depend on the fact that the amplitude of the periodic state is assumed to be small, we cannot expect the theory to be valid in a domain of parameter space where the amplitude may become large.

Because of the above-mentioned shortcomings of our methods we are now trying to develop numerical techniques to analyze the one-sided model. This study will provide us a means to compare our present results with those from a numerical simulation. An independent numerical study[13] of the full dynamical problem using finite element methods is also in progress.

ACKNOWLEDGMENTS

Both authors would like to acknowledge the help and guidance of Professor J. S. Langer in the preparation of this paper. They would also like to thank Professor R. F. Sekerka for many helpful conversations, and Dr. V. Datye and Dr. D. Kurtze for many enlightening conversations. This research was supported by the U.S. Department of Energy, under Contract No. DE-AM03-765-F00034.

APPENDIX A

We have

$$W^{(2)}(\vec{k}\mid\vec{k}_1,\vec{k}_2)=\psi/4\bar{v}(k-k_1-k_2)\ ,$$

$$W^{(3)}(\vec{k}\mid\vec{k}_1,\vec{k}_2,\vec{k}_3)=\psi^2/24\bar{v}\sum_i(k_j'^2+k_j-k_s)\times\left[\frac{\vec{k}_j'\cdot\vec{k}}{k}-k_j'\right],$$

where

$$k_i=\mid\vec{k}_i\mid\ ,$$

$$\vec{k}_i'=\vec{k}-\vec{k}_i\ ,$$

$$k_s=\sum_j k_j\ ,$$

and

$$\psi=\frac{1-\beta}{(1+\beta)}\ .$$

APPENDIX B

From Eq. (2.8) it is easy to see that

$$\vec{\nabla}_1 G(P\mid p_1)\cdot\hat{n}\,dS_1=\left[1+\frac{z-z_1}{2\tau}-\frac{\vec{\Delta x}\cdot\vec{\nabla}_1\xi_1}{2\tau}\right]\times G(p\mid p_1)d^2x\ .$$

The singularity arises from the $z-z_1$ term in the limit as $p\to p_1$. Consider the following integral:

$$I=\int_{-\infty}^{t}dt_1\int d^2x_1\frac{z-z_1}{2\tau}G(p\mid p_1)f(p_1)$$

in the limit as $z-z_1\equiv\epsilon\to 0$. Expanding $f(p_1)$ about p, we have

$$I=\int dt_1\frac{\epsilon}{2\tau}\frac{e^{-(\epsilon^2/4\tau)-\epsilon-\tau}}{(4\pi\tau)^{3/2}}\int d^2x_1\exp\left[-\frac{(\Delta\vec{x})^2}{4\tau}\right]\left[f(\vec{x},t)-\vec{\Delta x}\cdot\vec{\nabla}_1 f-\tau\frac{\partial f}{\partial t_1}+\cdots\right].$$

The spatial integrals are of the form

$$\int d^2x_1 e^{-(\Delta x)^2/4\tau}(\Delta\vec{x})^j\sim\tau^{1+(1/2)j}\ ,$$

therefore

$$I_j\sim\epsilon\int dt_1\tau^{(j-3)/2}e^{-(\epsilon^2/4\tau)-\tau}\underset{\epsilon\to 0}{\to}0\quad\text{if } j\neq 0\ .$$

Similarly, all integrals involving a nonzero power of τ from the expansion vanish in the limit as $\epsilon\to 0$. The only term that survives is the zeroth-order term:

$$I=2\pi\epsilon f(\vec{x},t)\int_{-\infty}^{t}dt_1\frac{e^{-(\epsilon^2/4\tau)-\tau}}{4(\pi\tau)^{3/2}}$$

$$=\tfrac{1}{2}f(\vec{x},t)\ .$$

Therefore the contribution from this singularity in the last term in Eq. (2.11) is

$$\tfrac{1}{2}[u(p^{\text{int}})-1]\ .$$

APPENDIX C

We have

$$B^{(1)}(k,\mid k,\omega)=2-1/\bar{v}-\xi k^2-\frac{1}{h}[2-E(1/v+\xi k^2)+i\omega]$$

where

$$h=(1+k^2+i\omega)^{1/2}$$

and

$$E=(1-2\kappa)\ .$$

We write

$$B^{(2)}(k,\omega\mid k_1,\omega_1,k_2,\omega_2)=\sum_{j=1}^{2}\tfrac{1}{2}i\omega_j\left[\frac{1}{h_j}-\frac{1}{h}[1-(1+E)/2\bar{v}]-\xi(1+E)k_j^2\right]$$
$$-\sum_{j=1}^{2}\tfrac{1}{2}(1/\bar{v}+\xi k_j^2)\left[h_j-h+\vec{k}'_j\cdot\frac{\vec{k}}{h}\right]$$
$$-\sum_{j=1}^{2}\left[1+\frac{1}{2h}-h_j+\tfrac{1}{2}(E/\bar{v}+E\xi k_j^2-1)\left[\frac{1}{h_j}-\frac{1}{h}\right]-\frac{1}{2}\frac{1}{h_j}\right]$$
$$-\left[1-\frac{E}{h}\right]W^{(2)}(k\mid k_1,k_2)\ ,$$

where

$$h_j=(1+k_j^2+i\omega_j)^{1/2}$$

and

$$\vec{k}'_j=\vec{k}-\vec{k}_j\ .$$

We then write

$$B^{(3)}(k,\omega\mid k_1,\omega_1,k_2,\omega_2,k_3,\omega_3)=\tfrac{4}{3}+\tfrac{1}{2}\xi k k_1k_2k_3\left[\frac{E}{h}-1\right]-\frac{1}{3}\left[\frac{1}{h}+3h\right]+\left[\frac{E}{h}-1\right]W^{(3)}(k\mid k_1,k_2,k_3)$$
$$-\frac{k^2}{3\bar{v}h}+\tfrac{1}{2}(1+E)\xi\sum_{j=1}^{3}\left[\frac{i\omega_j}{6}\right]\sum_{m\neq j}k_m^2\left[\frac{1}{h}-\frac{1}{h_{jm}}\right]$$
$$+E/6\bar{v}\sum_{j=1}^{3}\left[\frac{1}{h_j}+h_j-2\left[\frac{1}{h'_j}+h'_j\right]+\frac{1}{h}+h\right]$$
$$-\sum_{j=1}^{3}\tfrac{1}{6}i\omega_j\left[\frac{1}{h_j}+h_j+\frac{1}{h'_j}+h'_j-\tfrac{1}{2}(1+E)/\bar{v}\frac{1}{h'_j}\right]$$
$$+\frac{i\omega}{6}\sum_{j=1}^{3}\left[h'_j+\frac{1}{h'_j}-\tfrac{1}{2}(1+E)/\bar{v}\frac{1}{h'_j}\right]+1/3\bar{v}\sum_{j=1}^{3}\left[h_j+h-2h'_j+\frac{1}{2}\frac{k_j'^2}{h'_j}\right]$$
$$+\tfrac{1}{3}\sum_{j=1}^{3}W_{j'}^{(2)}\left[h-h'_j-\frac{kk_j}{h}+\frac{E}{h}-\frac{E}{h'_j}\right]$$
$$+\frac{\xi}{3}\sum_{j=1}^{3}\left[k_j^2\left[h+h_j-\frac{1}{2}\frac{kk'_j}{h}\right]-h'_j(k_s^2-k_j^2)+\frac{k_1k_2k_3k_j'^2}{k_jh'_j}\right]$$
$$+\frac{\xi E}{6}\sum_{j=1}^{3}\left[k_j^2\left[\frac{1}{h_j}+h_j+\frac{1}{h}+h\right]-(k_s^2-k_j^2)\left[\frac{1}{h'_j}+h'_j\right]\right]$$
$$+\tfrac{1}{3}\sum_{j=1}^{3}\left[\frac{1}{h'_j}+3h'_j-\frac{1}{h_j}-3h_j\right]+\frac{1}{2}\frac{(1+E)}{h}\sum_{j=1}^{3}i\omega_jW_{j'}^{(2)}\ ,$$

where

$$k_s^2=\sum_j k_j^2 ,$$

$$h_q'=[1+(\vec{k}-\vec{k}_q)^2+i(\omega-\omega_q)]^{1/2} ,$$

$$\vec{k}_q'=\vec{k}-\vec{k}_q ,$$

and

$$W_{j'}^{(2)}=W^{(2)}(k_{mn}\mid k_m,k_n) ,$$

and

$$j\neq m \text{ or } n .$$

APPENDIX D

We have

$$\alpha_3(k_0)=-\left.\frac{\partial B^{(1)}(k,\omega\mid k,\omega)}{\partial\omega}\right|_{\omega=0,\ k=k_0} ,$$

$$\alpha_4(k_0)=-i\left.\frac{\partial B^{(1)}(k,\omega\mid k,\omega)}{\partial k}\right|_{\omega=0,\ k=k_0} ,$$

$$\alpha_5(k_0)=-\frac{1}{2}\left.\frac{\partial^2 B^{(1)}(k,\omega\mid k,\omega)}{\partial k^2}\right|_{\omega=0,\ k=k_0} ,$$

$$\alpha_6(k_0)=-i\left.\frac{\partial B^{(2)}(k,\omega\mid k_1,\omega_1,k_2,\omega_2)}{\partial k_1}\right|_{\omega=\omega_1=\omega_2=0,\ k=k_1+k_2=k_0,\ k_1=2k_0,\ k_2=-k_0} ,$$

$$\alpha_7(k_0)=-i\left.\frac{\partial B^{(2)}(k,\omega\mid k_1,\omega_1,k_2,\omega_2)}{\partial k_1}\right|_{\omega=\omega_1=\omega_2=0,\ k=k_1+k_2=k_0,\ k_1=-k_0,\ k_2=2k_0} ,$$

$$\beta_3(k_0)=-\left.\frac{\partial B^{(1)}(k,\omega\mid k,\omega)}{\partial\omega}\right|_{\omega=0,\ k=2k_0} ,$$

$$\beta_4(k_0)=-i\left.\frac{\partial B^{(1)}(k,\omega\mid k,\omega)}{\partial k}\right|_{\omega=0,\ k=2k_0} ,$$

$$\beta_5(k_0)=-\frac{1}{2}\left.\frac{\partial^2 B^{(1)}(k,\omega\mid k,\omega)}{\partial k^2}\right|_{\omega=0,\ k=2k_0} ,$$

$$\beta_6(k_0)=-i\left.\frac{\partial B^{(2)}(k,\omega\mid k_1,\omega_1,k_2,\omega_2)}{\partial k_1}\right|_{\omega=\omega_1=\omega_2=0,\ k=k_1+k_2=2k_0,\ k_1=k_0,\ k_2=k_0} .$$

Using the expressions for $B^{(1)}$ and $B^{(2)}$ of Appendix C, we have that

$$\left.\frac{\partial B^{(1)}(k,\omega\mid k\omega)}{\partial\omega}\right|_{\omega=0,\ k=nk_0}=-\frac{1}{h_{n0}}+\frac{1}{2h_{n0}^2}(2-E/\bar{\nu}-\xi En^2k_0^2) ,$$

$$\left.\frac{\partial B^{(1)}(k,\omega\mid k\omega)}{\partial k}\right|_{\omega=0,\ k=nk_0}=-2\xi nk_0+\frac{nk_0}{h_{n0}^3}(2-E/\bar{\nu}-\xi En^2h_0^2)+\frac{2\xi Enk_0}{h_{n0}} ,$$

$$\left.\frac{\partial^2 B^{(1)}(k,\omega\mid k\omega)}{\partial k^2}\right|_{\omega=0,\ k=nk_0}=-2\xi+(2-E/\bar{\nu}-5\xi En^2k_0^2)\frac{1}{h_{n0}^3}$$

$$-\frac{3n^2k_0^2}{h_{n0}^5}(2-E/\bar{\nu}-\xi En^2k_0^2)+\frac{2\xi E}{h_{n0}} ,$$

$$\left.\frac{\partial B^{(2)}(k,\omega \mid k_n,\omega_n,k_m,\omega_m)}{\partial k_m}\right|_{\omega=\omega_1+\omega_2=0,\ \beta=1,\ k=k_n+k_m=0,\ k_n=nk_0,\ k_m=mk_0}$$

$$=-\xi m k_0\left[h_{m0}-h_{(n+m)0}+\frac{k_0^2 n(n+m)}{h_{(n+m)0}}\right]$$

$$-\tfrac{1}{2}(1/\bar{\nu}+\xi m^2 k_0^2)\left[\frac{mk_0}{h_{m0}}-\frac{k_0(n+m)}{h_{(n+m)0}}+\frac{nk_0}{h_{(n+m)0}}-\frac{n(n+m)^2k_0^3}{h^3_{(n+m)0}}\right]$$

$$-\tfrac{1}{2}(1/\bar{\nu}+\xi n^2 k_0^2)\left[-\frac{k_0(n+m)}{h_{(n+m)0}}+\frac{k_0(2m+n)}{h_{(n+m)0}}-\frac{m(n+m)^2k_0^3}{h^3_{(n+m)0}}\right]$$

$$-\left[\frac{k_0(n+m)}{2h_{(n+m)0}}-\frac{mk_0}{h_{m0}}+\frac{mk_0}{2h^3_{m0}}+\xi E m k_0\left[\frac{1}{h_{m0}}-\frac{1}{h_{(n+m)0}}\right]\right.$$

$$\left.+\tfrac{1}{2}(E/\bar{\nu}+\xi E m^2 k_0^2-1)\left[-\frac{mk_0}{h^3_{m0}}+\frac{(m+n)k_0}{h^3_{(n+m)0}}\right]\right]$$

$$-\left[\frac{k_0(n+m)}{2h_{(n+m)0}}+\tfrac{1}{2}(E/\bar{\nu}+\xi E n^2 k_0^2-1)\left[\frac{k_0(n+m)}{h^3_{(n+m)}}\right]\right],$$

where the above expression is multiplied by 2 if $m\neq n$ and

$$h_{n0}=(1+n^2k_0^2)^{1/2},$$

$$h_{(n+m)0}=[1+(n+m)^2k_0^2]^{1/2}.$$

[1]J. S. Langer, Rev. Mod. Phys. 52, 1 (1980).

[2]L. A. Tarshis, J. L. Walker and J. W. Ratter, in *Metallography, Structures, and Phase Diagrams,* 8th ed., edited by M. B. Beuer (American Society for Metals, Novelty, 1973), Vol. 8, p. 150.

[3]S. Chandrasekhar, *Hydrodynamic and Hydromagnetic Stability* (Dover, New York, 1981).

[4]D. J. Wollkind, and L. A. Segel, Trans. R. Soc. 51, 268 (1970).

[5]S. Strassler and W. R. Schneider, Phys. Condens. Matter 17, p. 153 (1974).

[6]G. E. Nash (unpublished).

[7]J. S. Langer and L. A. Turski, Acta Metall. 25, 1113 (1977).

[8]J. S. Langer, Acta Metall. 28, 777 (1977).

[9]W. W. Mullins and R. F. Sekerka, J. Appl. Phys. 35, 444 (1964).

[10]R. Mather, Ph.D thesis, Carnegie-Mellon University, 1981 (unpublished).

[11]A. C. Newell and J. A. Whitehead, J. Fluid Mech. 38, 379 (1969).

[12]G. T. Dee (unpublished).

[13]D. Kurtze (private communication).